Clim Dyn
DOI 10.1007/s00382-013-1861-2

Present and future near-surface wind climate of Greenland from high resolution regional climate modelling

W. Gorter · J. H. van Angelen · J. T. M. Lenaerts · M. R. van den Broeke

Received: 8 November 2012 / Accepted: 24 June 2013

Abstract The present and twenty-first century near-surface wind climate of Greenland is presented using output from the regional atmospheric climate model RACMO2. The modelled wind variability and wind distribution compare favourably to observations from three automatic weather stations in the ablation zone of southwest Greenland. The Weibull shape parameter is used to classify the wind climate. High values ($\kappa > 4$) are found in northern Greenland, indicative of uniform winds and a dominant katabatic forcing, while lower values ($\kappa < 3$) are found over the ocean and southern Greenland, where the synoptic forcing dominates. Very high values of the shape parameter are found over concave topography where confluence strengthens the katabatic circulation, while very low values are found in a narrow band along the coast due to barrier winds. To simulate the future (2081–2098) wind climate RACMO2 was forced with the HadGEM2-ES general circulation model using a scenario of mid-range radiative forcing of +4.5 W m^{-2} by 2100. For the future simulated climate, the near-surface potential temperature deficit reduces in all seasons in regions where the surface temperature is below the freezing point, indicating a reduction in strength of the near-surface temperature inversion layer. This leads to a wind speed reduction over the central ice sheet where katabatic forcing dominates, and a wind speed increase over steep coastal topography due to counteracting effects of thermal and katabatic forcing. Thermally forced winds over the seasonally sea ice covered region of the Greenland Sea are reduced by up to 2.5 m s^{-1}.

Keywords Greenland · RACMO2/GR · Katabatic · Weibull · Wind

1 Introduction

The Greenland ice sheet (GrIS) is the largest body of ice on the Northern Hemisphere, equivalent to 7.3 m of sea level (Bamber et al. 2001). In response to global climate change, an increasing rate of GrIS mass loss has been observed (Rignot et al. 2011), which is about equally split between surface processes and ice dynamics (Van den Broeke et al. 2009). To understand these processes and predict future changes thereof, it is necessary to consider mass exchanges at the surface, which are strongly coupled to the wind climate.

Driving forces of the near-surface wind can be split into large-scale forcing and local boundary layer processes (Van den Broeke and Van Lipzig 2003). Low pressure systems from the North Atlantic storm track produce relatively higher rates of precipitation along the southeastern and western coasts (Dethloff et al. 2002). The net effect of these passing systems is the climatological Icelandic Low to the southeast of the ice sheet. Large-scale synoptic systems are disturbed by the topography and size of the GrIS, giving rise to various interesting circulation patterns such as tip jets near Cape Farewell (Våge et al. 2009). The GrIS boundary layer is characterised by a surface temperature inversion that is strongest in winter, but persists year-round (Cassano et al. 2001; Duynkerke and van den Broeke 1994). This inversion is predominantly caused by a

Electronic supplementary material The online version of this article (doi:10.1007/s00382-013-1861-2) contains supplementary material, which is available to authorized users.

W. Gorter (✉) · J. H. van Angelen · J. T. M. Lenaerts · M. R. van den Broeke
Institute for Marine and Atmospheric Research (IMAU), Utrecht University, Utrecht, The Netherlands
e-mail: w.gorter@uu.nl

Published online: 09 July 2013

negative surface radiation balance, and a resulting downward sensible heat flux that cools the near-surface air. The negative buoyancy of this layer creates a horizontal pressure gradient in the downslope direction that drives persistent and uniform katabatic winds (Klein et al. 2001). These winds are deflected in the cross-slope direction by the Coriolis force, while friction limits the speed and maintains a downslope component. Several field campaigns to study the katabatic wind have been carried out (e.g. Van den Broeke et al. 1994; Heinemann 1999; Steffen and Box 2001) showing that katabatic forcing is generally dominant over the ice sheet, except in summer, when the large scale forcing may become important (Heinemann and Klein 2002).

Horizontal variations in the height and strength of the temperature inversion layer give rise to thermal wind effects in the surface layer. The strength of the surface temperature inversion layer can be quantified using the concept of potential temperature deficit, which is defined as the difference between the actual potential temperature, and that of the free atmosphere, when extrapolated to the surface. The layer of cold air at the surface is then characterised by a potential temperature deficit, and will be referred to as the "temperature deficit layer" hereafter. Because air density is strongly determined by temperature, surface pressure is influenced by the vertically integrated potential temperature deficit. This effect is generally strongest over rough topography, where the height of the temperature deficit layer increases in the downslope direction, leading to a thermal pressure gradient force in the upslope direction. If the top of the temperature deficit layer is flat, thermal wind forcing is equal and opposite to the katabatic forcing (Van den Broeke and Van Lipzig 2003). Van Angelen et al. (2011b) showed that thermal winds are the primary transport mechanism of sea ice into the North Atlantic through Fram Strait, and crucial in understanding and predicting the seasonal sea ice cover along the east coast of the GrIS. Furthermore, thermal forcing gives rise to strong barrier winds that develop along the coast in the presence of strong temperature gradients that result from the large scale flow (Moore and Renfrew 2005; Van den Broeke and Gallée 1996).

Because of the harsh and remote environment, observational campaigns face technical difficulties which limit the temporal and spatial coverage of measurements on the GrIS. Significant improvement of spatial coverage has been realised through the setup of a network of Automatic Weather Stations (AWS) on and around the ice sheet. These stand-alone measurement devices continuously monitor near-surface temperature, wind speed, humidity, radiation balance and other variables. Most notably, the Greenland Climate Network (GC-net) consists of 15 AWS covering most geographical regions of the ice sheet (Steffen and Box 2001), the Danish Meteorological Institute maintains a network of AWS in the surroundings of the ice sheet (Cappelen et al. 2001), the Institute for Marine and Atmospheric Research of Utrecht University (UU/IMAU) maintains a transect of AWS across the ablation zone in southwest Greenland (Van den Broeke et al. 2008b), and recently the Geological Survey of Denmark and Greenland (GEUS) started the Programme for Monitoring of the Greenland Ice Sheet (PROMICE) which currently consists of 14 AWS in the Greenland ablation zone (Van As et al. 2011). Despite these improvements, these data only extend roughly 20 years back and large areas for which no measurements are available exist. This gap is partially filled by the large scale atmospheric reanalyses ERA-40 and ERA-interim from the European Centre for Medium-Range Weather Forecasts (ECMWF), which provide physically based interpolation and integration of a wide range of existing data (Dee et al. 2011). Because the width of the Greenland ablation zone ranges from a few km to more than 100 km (Bøggild et al. 2010), the resolution of the reanalyses is insufficient to capture the complex processes in this region. To circumvent this problem, the use of regional climate models (RCMs) that provide data with high spatial resolution is increasingly popular. Examples of these models include the Modèle Atmosphérique Régional (MAR) with 25 km resolution (Gallée and Schayes 1994; Franco et al. 2012), the Regional Atmospheric Climate Model version 2.1 (RACMO2) with 11 km resolution (Van Meijgaard et al. 2008), and the Polar MM5 with 24 km resolution (Box et al. 2009).

Several studies have investigated the characteristics of the wind distribution over the ocean using the two-parameter Weibull distribution as a convenient tool to characterise both wind speed and variability (Pryor et al. 2005; Monahan 2006b; Isemer and Hasse 1991). However, these studies were based on scarce observational data or on coarse reanalysis data and none of them have included the GrIS and surrounding seas. Sanz Rodrigo et al. (2012) evaluated the quality of the ECMWF reanalyses and output from RACMO2 against a large set of AWS on Antarctica, again using the Weibull distribution as a tool to quantify the properties of the wind distribution. The wind distribution in the high-resolution RACMO2 model was considerably improved relative to the distribution provided by the coarser reanalysis data. Previously, RACMO2 was used over the GrIS to give a detailed account of the near-surface climate (Ettema et al. 2010a) and the momentum budget (Van Angelen et al. 2011a).

Here, we present the wind climate of the GrIS and surroundings from high-resolution (11 km) RACMO2 model simulations, and we provide a description of the wind climate in terms of the Weibull parameters. To evaluate model performance, the results are compared with

data from three AWS in the ablation zone of southwest Greenland. Because a more exhaustive evaluation of RACMO2 already exists, here only a limited evaluation focusing on the wind distribution is presented. Furthermore, we present for the first time projected changes in average wind speed and wind variability by comparing model simulations for the period 1981–1998 with those for 2081–2098, following a scenario of mid-range warming developed for the next Intergovernmental Panel on Climate Change assessment report (AR5).

2 Data and methods

2.1 Observations from AWS

The observational data used in this study originate from three AWSs in the ablation zone of southwest Greenland. These AWS from the Institute for Marine and Atmospheric Research Utrecht (IMAU) are part of the K-transect near Kangerlussuaq that was set up in 1990 as part of the Greenland Ice Margin Experiment. The transect consists of a line of mass balance measurements along the 67°N latitude, ranging from the ice edge to an elevation of 1,800 m above sea level (Oerlemans and Vugts 1993; Van de Wal et al. 2012). The three AWSs were added to the K-transect in 2003 at three locations known as S5, S6 and S9 in order of progressing distance from the ice edge. Table 1 summarises the details of the AWS locations.

The AWSs are located in different climatic regions of the ablation and percolation zone. The surface at S9 is smooth, and covered with a layer of wet snow throughout the summer, while the surface at S5 is free of snow in summer and covered in a thin layer of snow in winter. Furthermore, the terrain at S5 and to a lesser extent S6 is covered with ice hummocks that cause a rough surface topography. The AWS are mounted on four legs that make a small angle with the horizontal and stand on the surface, so that they are allowed to sink with the lowering surface during the ablation season. Furthermore, the AWSs are equipped with sensors for temperature, specific humidity, wind speed, wind direction, pressure, and sensors that measure the radiation budget. The radiative fluxes are measured at 6 m height, wind speed and direction, temperature and humidity are measured at both 6 and 2 m height, and pressure is measured in the electronics box. The 10 m wind speed was determined using Monin–Obukhov similarity theory, while observed 10 m wind direction was taken equal to 6 m wind direction. Van den Broeke et al. (2008a) present an overview of all the individual sensors, their accuracy and mean values of measured variables. Hourly AWS data for the period 2003–2010 were used throughout this study. All data were quality checked before use, removing events of sensor freeze-up and other spurious data (Van den Broeke et al. 2008a).

Table 1 Elevation and distance from the ice edge of the AWS used in this study

	S5	S6	S9
Elevation (m ASL)	490	1,020	1,520
Ice edge (km)	3	38	88
Latitude	67°06′N	67°05′N	67°05′N
Longitude	50°07′W	49°23′W	48°14′W

2.2 The RACMO2 regional climate model

The Regional Atmospheric Climate Model version 2.1 (RACMO2) used in this study, was developed by the Royal Netherlands Meteorological Institute (KNMI) (Van Meijgaard et al. 2008) and consists of the semi-Lagrangian dynamics kernel of the numerical weather prediction model HiRLAM (Undén et al. 2002), complemented with the physics package of the European Centre for Medium-Range Weather Forecasts Cycle 23r4 (White 2001). It was adapted for use in the polar regions by the UU/IMAU. The model has been shown to realistically simulate the surface mass balance of Greenland (Ettema et al. 2009) and Antarctica (Lenaerts et al. 2012b). Furthermore, it was used to investigate the near-surface climate and extensively evaluated against observations from AWS on the GrIS (Ettema et al. 2010b). The model includes a multi-layer snow scheme that includes the effects of meltwater percolation, retention and refreezing (Bougamont et al. 2005). A new snow albedo scheme has also been included in the model, which treats the effects of dry and wet snow metamorphism on snow grain size, and improves the modelled length of the melt season (Kuipers Munneke et al. 2011). Finally, a drifting snow routine has been added to the model (Lenaerts et al. 2012a). Wind speeds at the 10 m standard level are calculated from the lowest model level using stability corrections to allow comparison with other data.

The model domain comprises the GrIS and surrounding seas, including parts of the Canadian Arctic, Svalbard and Iceland. The model has 40 hybrid vertical levels. Surface layer values of variables are calculated using similarity theory. The horizontal model domain has 306 × 312 grid points, which translates to a resolution of roughly 11 km. This high horizontal resolution is essential for capturing small scale variations in the ablation zone where complex topography and surface type variations influence the local climate.

For the evaluation of the present day climate, the model is forced every 6 h at the lateral boundaries by observationally based ECMWF reanalyses ERA-40 (1960–1988)

and ERA-interim (1989–2011). Sea ice extent and sea surface temperature are prescribed from the reanalyses to ensure accurate surface conditions. Finally, bare ice albedo in the ablation zone is prescribed from remote sensing measurements from the MODerate resolution Imaging Spectroradiometer to capture the variability in the ablation zone (Van Angelen et al. 2012). The interior model domain is allowed to evolve freely, and is therefore independent of observations. To study projected changes of the wind climate, the model is forced with output from the HadGEM2 General Circulation Model for 1970–2098 at the lateral boundaries and the ocean-atmosphere interface. Bare ice albedo is fixed at a value of 0.45. For future simulations after 2004, HadGEM2 is forced with a scenario of mid-range warming known as the Representative Concentration Pathway 4.5 (RCP4.5) that was developed for the next IPCC assessment report. This scenario assumes an increase of radiative forcing relative to pre-industrial values of +4.5 W m^{-2} at stabilisation after 2100 (Moss et al. 2010).

2.3 Evaluation of the wind climate

The near-surface climate including the annual average wind speed from RACMO2 has been extensively evaluated against a large set of AWS for an older version of the model (Ettema et al. 2010b). This evaluation showed that RACMO is capable of realistically simulating the average near-surface climate and wind field. The narrow ablation zone is characterised by strong gradients and topographic differences, and is therefore the region where model resolution is most critical. Good performance of the model in this region gives confidence that the rest of the ice sheet is well represented, as confirmed by earlier evaluations. As a result, we limit our present evaluation to a comparison of model results with three AWS in the ablation zone in southwest Greenland, focussing particularly on the distribution of wind speed and wind direction. An inverse distance-squared algorithm was used to interpolate RACMO2 data from the model grid to the locations of the AWS. It should be kept in mind that the evaluation presented here covers a small region, which is not representative of all other areas of the GrIS.

The frequency distribution of wind speeds is a very valuable tool to characterise the wind regime. A narrow distribution implies a relatively constant forcing, such as a katabatic forcing, while a wide distribution indicates variable (synoptic) forcing (Renfrew and Anderson 2002). To facilitate comparison between the distributions at different locations, it is convenient to fit the data to the two-parameter Weibull distribution (Pavia and O'Brien 1986):

$$F(V) = \frac{\kappa}{\lambda}\left(\frac{V}{\lambda}\right)^{\kappa-1} exp\left(-\left(\frac{V}{\lambda}\right)^{\kappa}\right) \quad (1)$$

where $F(V)$ is the frequency distribution of wind speeds, V is the modulus of the wind speed, κ is the shape parameter and λ is the scale parameter. λ is linearly related to the annual mean wind speed V_{avg} through:

$$\lambda = \frac{V_{avg}}{\Gamma\left(1+\frac{1}{\kappa}\right)} \quad (2)$$

where Γ is the complete gamma function. λ generally lies very close to the mean wind speed and will be used as an indicator thereof. The value of the shape parameter determines whether the distribution is narrow or wide. High values ($\kappa > 4$) represent a narrow distribution with a short tail, such that winds are very uniform and high wind events are rare. These winds tend to derive from a very constant forcing mechanism, such as the katabatic forcing. Contrastingly, the shape of the wind distribution is wide and long-tailed for low values of the shape parameter ($\kappa < 2$). This is representative of wind regimes of more variable forcing and more frequent high wind speed events. A value of $\kappa = 3.6$ represents approximately a symmetrical Gaussian distribution. Methods of differing complexity exist to determine the best-fit Weibull parameters, but negligible differences are generally found between them (Monahan 2006a). Therefore, the standard method of least squares is used to fit the distribution to the available data.

3 Results

3.1 Evaluation of model performance

To evaluate the performance of RACMO2 in simulating the near-surface wind climate, the modelled and observed 10 m wind speed frequency distributions for 2004–2009 are shown in Fig. 1. At S6 and S9 the wind speed is very well represented in RACMO2 and shows minimal deviations from observations as further shown in Table 2. Here, the model is able to capture differences in the terrain which show up in the lower wind speed at S6. For S6, the model bias is small compared to the range of variability. This is also true for S9, although a small negative wind speed bias is simulated here, which is also seen at S5. At S5, the relative frequency of low wind speeds is overpredicted by the model while the relative frequency of high wind speeds is underpredicted. One explanation for this is that the position of S5 near the front of Russell Glacier is not well resolved by the model topography, despite the relatively high resolution. Another possible explanation is that RACMO2 overestimates the surface friction through an overestimation of the surface roughness length for momentum. Considering that aside from some inaccuracies at this location of complex topography, RACMO2 is able

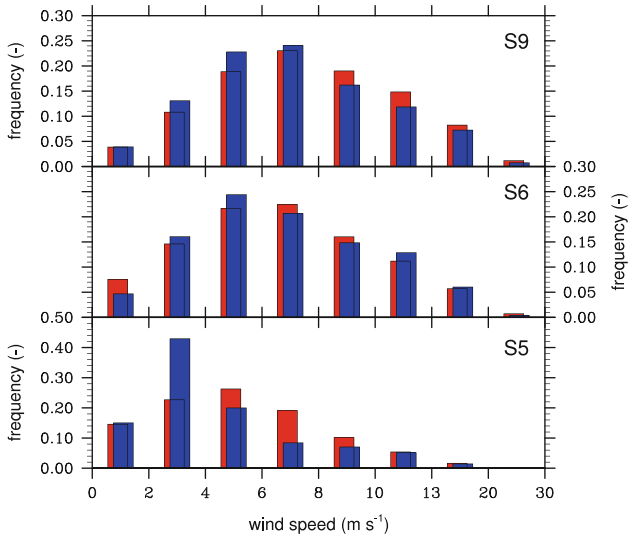

Fig. 1 Frequency distributions of 10 m windspeed (m s^{-1}) of all three AWS. Both observations (*red*) and RACMO2 results (*blue*) are shown. A inverse distance squared algorithm was used to interpolate RACMO2 data to the desired location. Mean hourly wind speeds from 2004 to 2009 are used from the AWS, while three hourly instantaneous wind speeds from RACMO2 are used

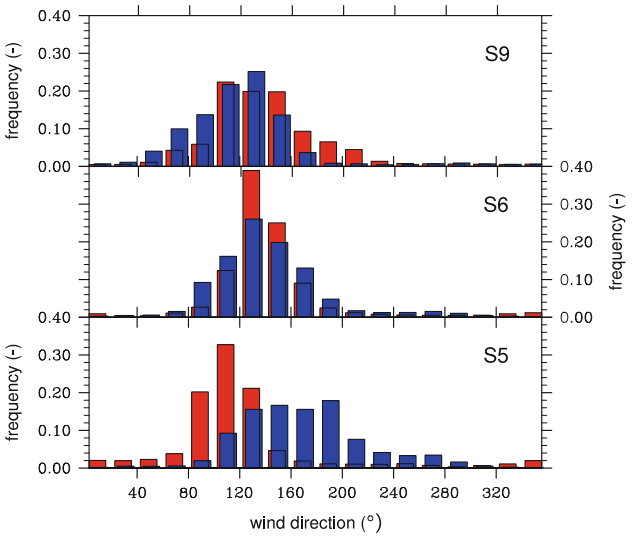

Fig. 2 Frequency distributions of 10 m wind direction at the locations of the three AWS. Obervations (*red*) and RACMO2 (*blue*) results are shown. Mean hourly data from the AWS, and three hourly data from RACMO2 was used from the period 2004–2009

Table 2 Comparison statistics between RACMO2 and observations from the K-transect, based on data from 2004 to 2009. The standard deviation is presented from RACMO2 data

	S5	S6	S9
Mean Obs. Wind (m s^{-1})	5.28	6.58	7.86
Mean Mod. Wind (m s^{-1})	4.40	6.72	7.32
Mean Bias (m s^{-1})	−0.87	0.14	−0.54
RMSE (m s^{-1})	2.04	1.87	2.03
SD (m s^{-1})	2.48	2.89	3.29

to provide a reasonable description of wind speed at the three stations. We conclude that the wind speed distribution in the ablation zone is generally realistically modelled.

Figure 2 presents the modelled and observed frequency distribution of 10 m wind direction for 2004–2009. Again, distributions at the locations S6 and S9 further from the ice edge are well represented and S5 shows considerable discrepancies. A small model bias of wind direction is found at S9 (−19.9°), which is well within the range of variability and on the order of the accuracy of the sensors. No model bias of the wind direction was found at S6, but variability was overpredicted. At S5, the spread of modelled wind direction is too large, and the dominant wind direction is biased. The observed variability of wind direction may be smaller than the predicted because of small scale topographic features that are not resolved by the model. This may also explain part of the bias of the average wind direction.

To gain insight into the ability of RACMO2 to resolve the seasonal cycle, short-term variability and extreme events, the daily average modelled and observed 10 m wind speed for the year 2004 are presented in Fig. 3. A summary of model performance is presented in Table 2. Wind speeds are well represented at S9 with a model bias and RMSE considerably smaller than the modelled standard deviation. Seasonal bias does not vary significantly over the year, indicating that RACMO2 realistically simulates the yearly cycle. At S6, the model performs even better. The mean bias and RMSE are smaller at S6, and are again considerably smaller than the modelled standard deviation. At S5 the 2004–2009 mean bias is −0.87 m s^{-1}, but at this location the bias is not constant over the year, and a clear summer mean bias of −1.46 m s^{-1} is observed. RACMO2 therefore overestimates the magnitude of the seasonal cycle at S5. Possibly this is related to enhanced contrasts between the ice sheet and nearby tundra in summer. Particularly at S6 and S9, a clear seasonal cycle is observed, with higher wind speeds and larger variability in winter and considerably lower wind speeds in summer. This seasonal cycle closely follows the strength of the katabatic forcing, which is strongest in winter. The low summer variability can partly be explained by a surface temperature that is limited to the melting point and therefore constrains temperature variations of the near-surface air and the strength of the katabatic forcing. Modelled wind speed variation on a timescale of days agrees well with observations, and RACMO2 is able to capture strong wind events lasting no more than a day. Not all extreme events are captured by the model, but considering it is allowed to evolve freely in the interior domain the observed deviation from observations is small. Remaining biases result from the poorly known spatial and temporal patterns of

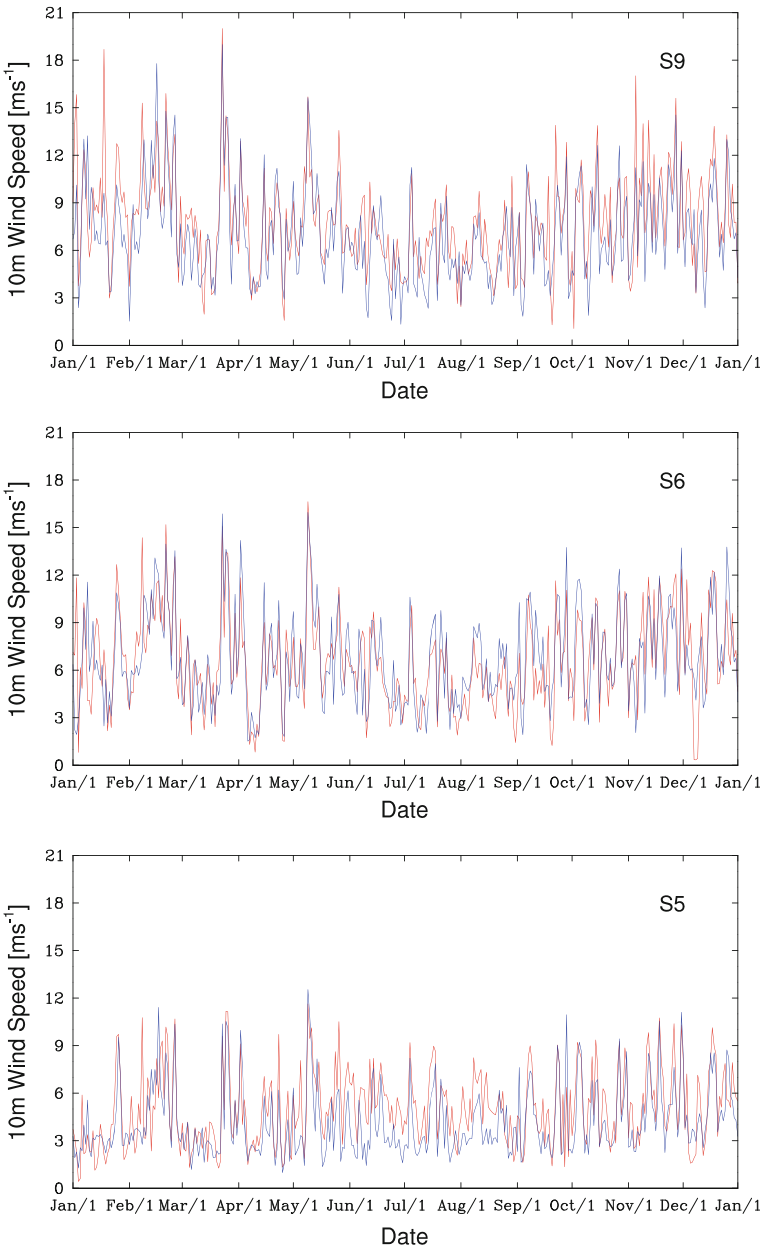

Fig. 3 Time series of daily averaged observed (*red*) and modelled (*blue*) 10 m wind speed (m s^{-1}) at three AWS locations for selected year 2004

roughness length and poorly defined stability corrections during very stable conditions that regularly occur in winter (Bromwich et al. 2001).

According to RACMO2, strong climatic gradients in wind speed exist over the ablation zone where the AWS are located. Figure 4 shows the average 10 m wind speed and direction in the region of the AWS in southwestern Greenland for the years 1960–2011. Wind speeds range from less than 2 m s^{-1} over the summer tundra to 10 m s^{-1} over the higher regions of the ice sheet in winter where the surface is smooth and strong katabatic winds develop. The model resolution is sufficient to capture the spatial scale of variations of the average wind field in this region and underlines the strong gradients near the ice margin. Over the tundra and the lower ablation zone the spatial scales of variation are very small, and the model resolution is not sufficient to resolve all topographic features. Since we present here the average wind climate we do not concern ourselves with these small-scale features that are of little influence on the average state (Van Angelen et al. 2011a).

3.2 Present day wind climate

An anti-cyclonic wind pattern persists over the GrIS throughout the year, as shown in Fig. 5, which shows average wind speed and direction for the years 1960–2011. This illustrates the quasi-permanent nature of the katabatic

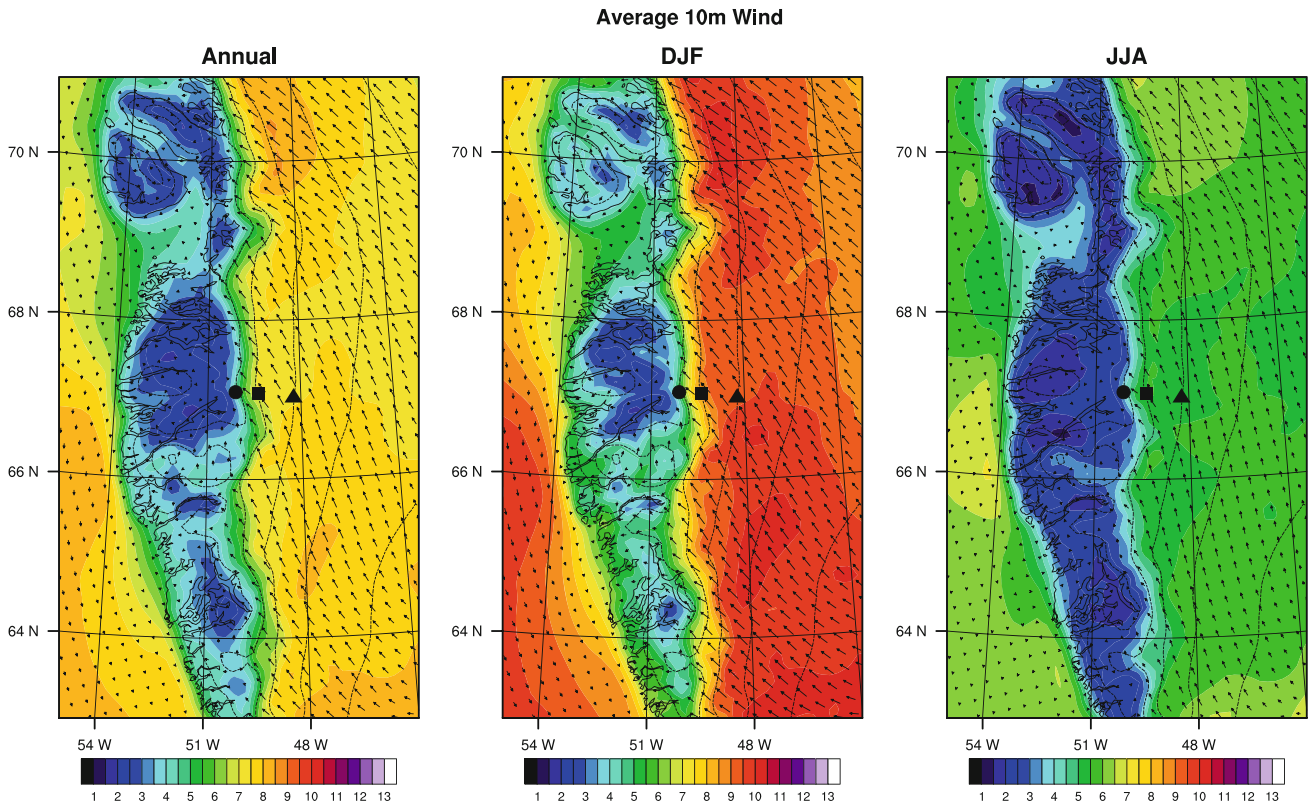

Fig. 4 10 m Wind speed (m s^{-1}) and direction in the region of the AWS in southwestern Greenland from daily average data for the period 1960–2011. Wind direction vectors represent vector average wind velocity vector. AWS sites are indicated with a *black circle* (S5), *square* (S6) and *triangle* (S9). From left to right the panels represent annual average, winter (DJF) average, and summer (JJA) average

winds that create a circulation that is deflected downslope of the height contours through the effects of friction. Relatively low wind speeds (5–8 m s^{-1}) are found over the interior ice sheet, since in the absence of a significant surface slope katabatic forcing is weak. Wind speeds increase towards the margins as the surface slope increases, and average wind speeds of up to 10 m s^{-1} are found over large regions in west and south Greenland during winter. Over the west coast of the GrIS the large scale pressure gradient acts in the same direction as the katabatic forcing such that a persistent southerly jet of high wind speeds exists (Van Angelen et al. 2011a). The strongest winds are found in Dronning Louise Land in the northeast, where very cold conditions are combined with a large surface slope. The wind shows a pronounced seasonal cycle that is due to the katabatic forcing. A strongly negative surface radiation balance is observed in winter, such that the surface cools. This is compensated by a sensible heat flux from the air to the surface, which cools the near-surface air. Because this forcing is very strong and constant in time, strong katabatic winds result. In summer, the radiation balance is positive over most of the ice sheet, except the high and northern areas where surface albedo is very high (Box et al. 2006). Furthermore, air temperatures are mostly higher than surface temperatures because the surface is limited to the melting point (Duynkerke and van den Broeke 1994). Therefore, during summer the surface energy balance is closed by a positive radiation balance, a positive sensible heat flux and a negative latent heat flux or melt. The potential temperature deficit that results from this sensible heat flux is much smaller than in winter, and the modelled wind speeds reflect that.

In the absence of a large surface slope the cold air from the ice sheet accumulates over the tundra, a phenomenon known as cold air pooling. Cold air pooling can lead to strong temperature contrasts and associated thermal winds. This phenomenon acts over the sea ice covered western part of the Greenland Sea and Fram Strait. Very cold air from the northeast of the GrIS pools over this sea ice, which insulates the air from the warm sea. A strong east-west temperature contrast is set up that drives the northerly Greenland Sea Jet that can be linked to the transport of sea ice into the North Atlantic (Van Angelen et al. 2011b). In summer, sea ice is absent from the Greenland Sea, and wind speed is strongly reduced in the absence of thermal forcing (Fig. 5).

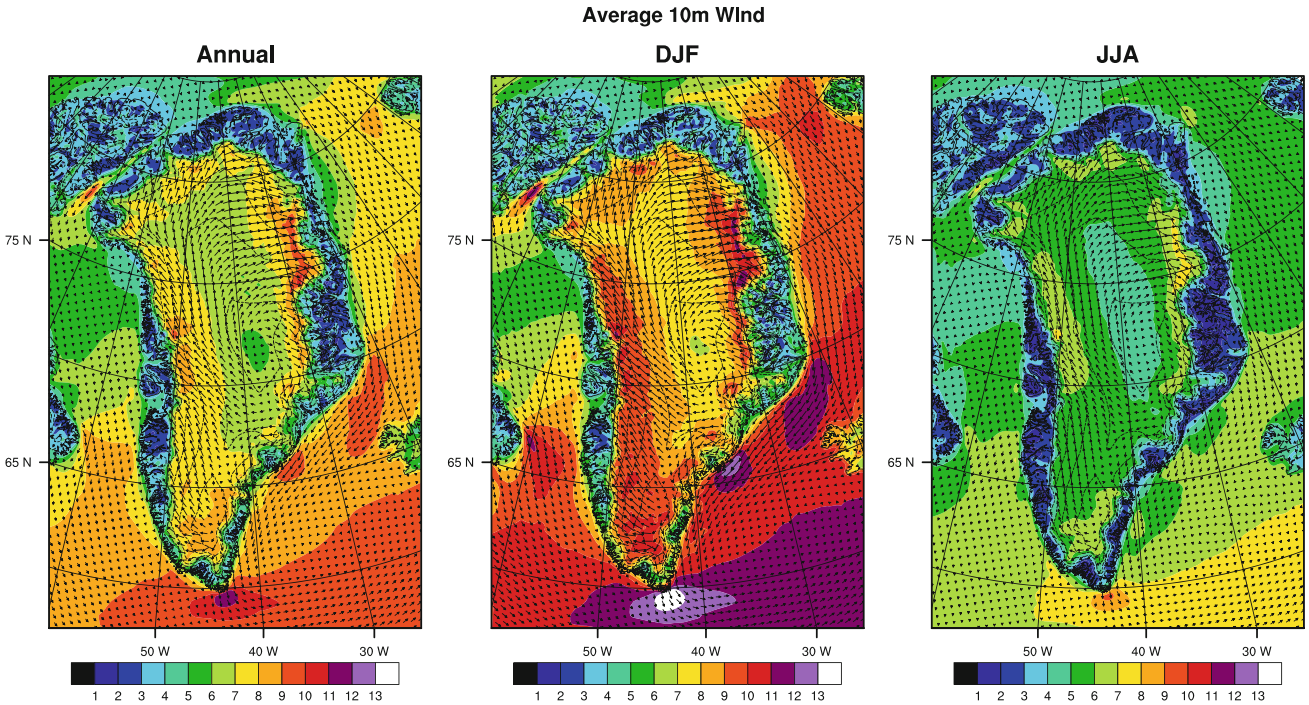

Fig. 5 10 m Wind speed (m s^{-1}) and direction over the Greenland ice sheet and surrounding seas from daily average data for the period 1960–2011. Wind direction vectors represent vector average wind velocity vector. From left to right the panels represent annual average, winter (DJF) average, and summer (JJA) average

The southeast coast of the GrIS is characterised by strong winds in response to the presence of the Icelandic Low which causes air flow along the coast (Fig. 5). Air is forced towards steep topography by the large scale circulation. Because it cannot rise over this topography, a pressure gradient builds that drives flow along the coast instead (Harden and Renfrew 2012). This mechanism of large scale forcing is further enhanced by thermal effects. The average wind direction shown in Fig. 5 also indicates the direction of average atmospheric mass transport. Along the southeast coast these arrows show a distinct pattern parallel to the coast, whereas hardly any mass transport occurs in the region of tip jets near Cape Farewell despite the high wind speeds. This difference is related to the directional constancy of the wind.

Directional constancy is defined as the ratio of the vector mean wind speed to the scalar mean wind speed:

$$DC = \frac{\left(\overline{u}^2 + \overline{v}^2\right)^{\frac{1}{2}}}{\overline{\left(u^2 + v^2\right)^{\frac{1}{2}}}} \tag{3}$$

Here, u and v are the components of the wind in easterly and northerly direction respectively. A directional constancy of 0 signifies winds with random direction, while a directional constancy of 1 indicates winds of uniform direction. A very high directional constancy of 0.8 or higher is found over most of the ice sheet, with the exception of the two domes and the ice ridge running over the ice sheet (Fig. 6). Here, in the absence of a surface slope the katabatic forcing is weak and winds are controlled by synoptic processes, which are much more variable in direction. Extremely high values (>0.95) are found in regions of strong katabatic winds in the north near the ice sheet edge. Surprisingly uniform winds are found along the southeastern coast. These are a direct result of the average large scale forcing associated with the presence of the Icelandic Low, and the presence of the ice sheet which acts as an orographic barrier. Over the ocean, a directional constancy of 0.4 or lower is observed for most regions, except the seas east of the GrIS where thermal forcing is a stabilising factor. Directional constancy is therefore a useful tool to give a broad classification of the wind regime and the associated forcings, as it clearly discriminates between regions of katabatic forcing and synoptic forcing.

In this manner, wind direction can be used to provide insight into the driving processes of the wind and to characterise the wind climate without the need for an elaborate analysis of the terms of the momentum budget. Complementary to this analysis, a classification of wind speed and variability can be made through a Weibull analysis. Figure 7 shows the application of the Weibull analysis to the modelled and observed wind field at S9. As noted in Sect. 3.1, the low wind speeds are slightly overestimated by RACMO2, leading to a small negative model

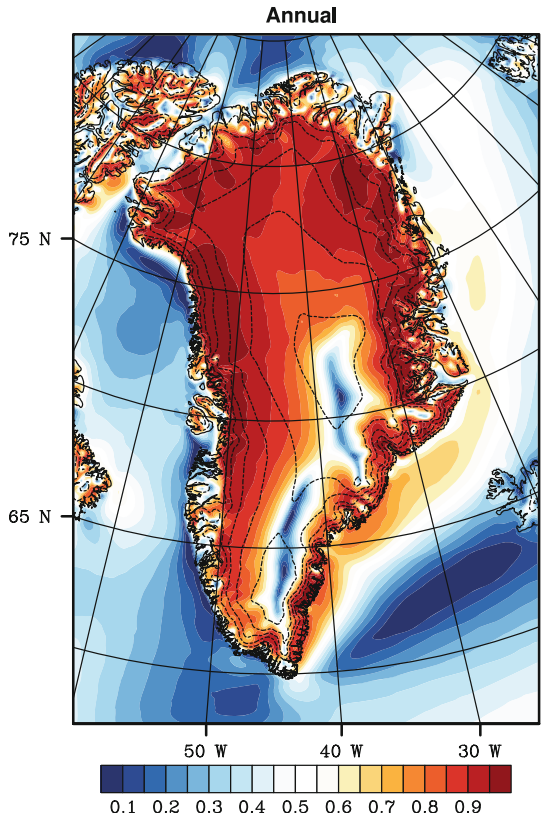

Fig. 6 Directional constancy (–) of the 10 m daily average wind for the period 2004–2009

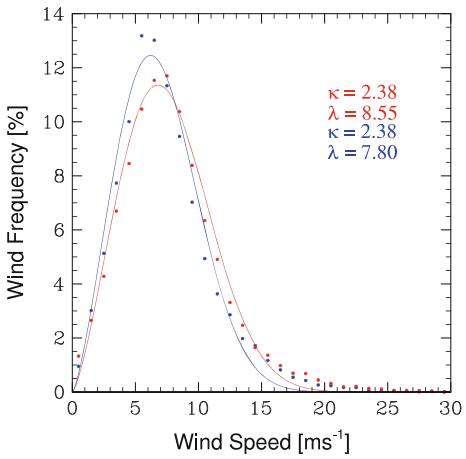

Fig. 7 Two-parameter Weibull distribution of observed (*red*) and modeled (*blue*) 10 m wind speeds at S9. Wind speeds are binned in 1 m s^{-1} intervals (*dots*). The fitted Weibull distribution is shown as a *solid line*. The fitted values of the shape parameter κ and the scale parameter λ are shown

bias at S5 and S9, but the overall performance of the model is good. In particular, we note that the model appears able to accurately resolve the shape parameter κ. Even at S5 and S6, where the terrain is more challenging to model, modelled values of the shape parameter κ deviate only from observations by 0.01 (not shown). Differences in the scale parameter λ are larger by up to 1 m s^{-1}.

Maps of the scale parameter of the Weibull distribution (Fig. 8) closely follow the patterns of wind speed presented in Fig. 5 as they are related through Eq. (2). Because of this the scale parameter is not very discriminating and yields little new information. The shape parameter varies significantly over the modelled region and is therefore more discriminating (Fig. 8). For the value $\kappa = 3.6$, the wind distribution has a symmetrical Gaussian shape. Locations where the shape parameter is high ($\kappa > 4$) are characterised by a narrow distribution with low wind speed variability and a low frequency of high wind speed events. Locations where $\kappa < 2$ are characterised by a long-tailed right-skewed distribution with a large windspeed variability and a high frequency of high wind speed events.

Over the ocean, a shape parameter of roughly $\kappa = 3$ is observed, which, compared to a typical mid-latitude value of $\kappa = 2$, signifies more constant winds at high latitudes with fewer extreme events. Near the coast a clear band of variable winds is present where $\kappa < 2$. This is the signature of strong barrier winds near the coast (Moore and Renfrew 2005). Over the ice sheet the shape parameter is higher, which is a result of the constant nature of the katabatic forcing which creates relatively uniform winds. The absence of strong katabatic forcing over the two ice domes and the ridge in between is reflected in the value of κ that is approximately the same as that over the ocean, underlining the synoptic influence in this region. Interestingly, the value of κ over the sloped surface of the southwest is surprisingly low, considering the significant katabatic forcing in the area. In this region the spatial distribution of the shape parameter shows a very different pattern than the directional constancy (Fig. 6), underlining the complementary nature of the two. The low value of κ is likely a result of the synoptic activity associated with passing low pressure systems over the southern part of the GrIS or the occurrence of barrier winds in summer (Van den Broeke and Gallée 1996). High values of the shape parameter (>4) occur to the north where the potential temperature deficit is stronger and katabatic winds dominate most of the year. Extreme values (>5) occur in the north in regions of concave topography, where katabatic air flows show confluence. In regions without confluence, the supply of negatively-buoyant air poses a limitation to the persistence of katabatic flow (Parish and Bromwich 1987). Due to confluence of the flow, the cold air drainage basin is enlarged, increasing the intensity and persistence of katabatic winds and reducing the adiabatic heating (Van de Berg et al. 2008). As a result, some of the most uniform winds on Earth are created, only rivalled by those in Antarctica where a similar pattern was found (Sanz Rodrigo et al. 2012). Over convex topography, the opposite

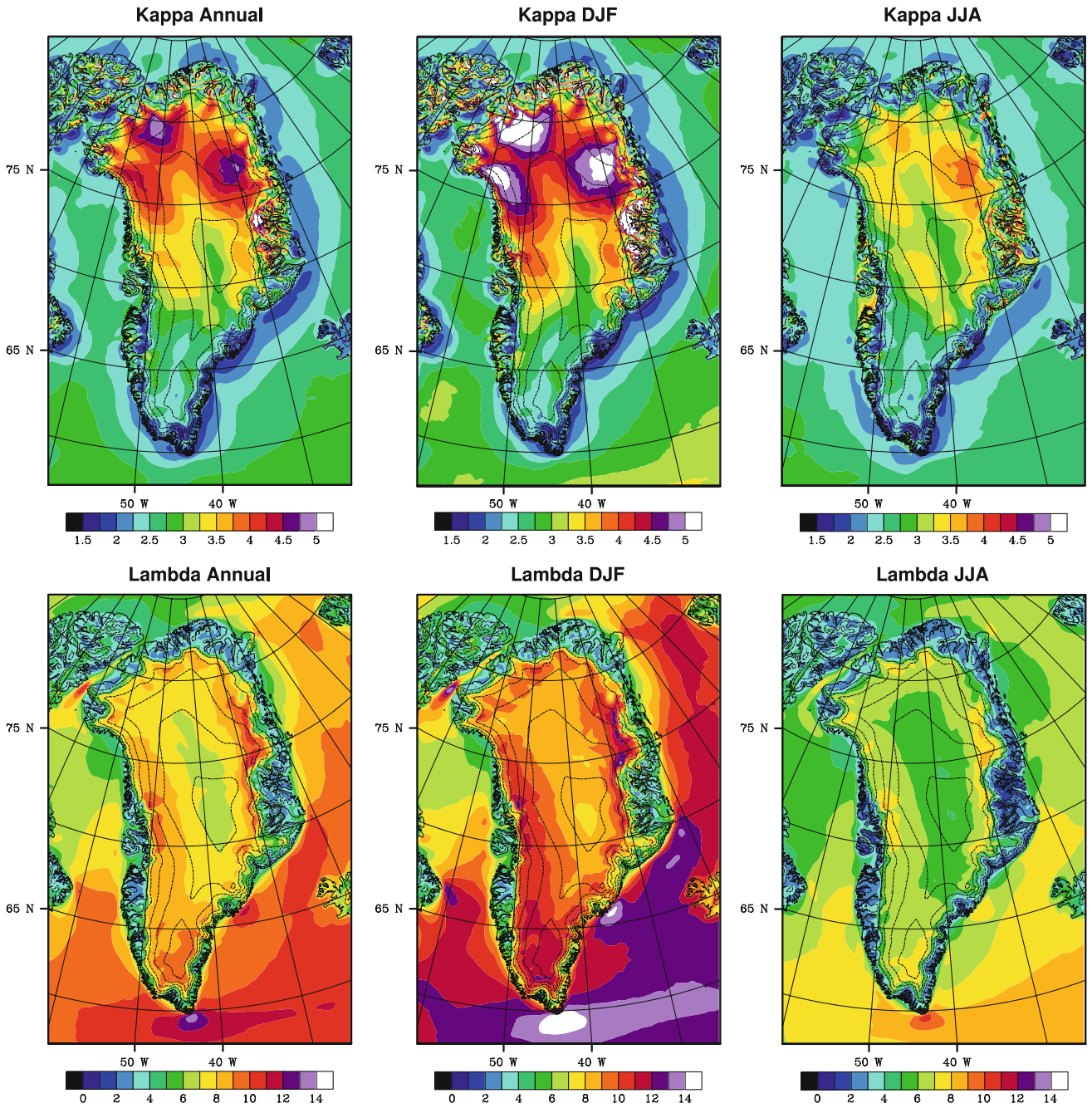

Fig. 8 Map of Weibull parameters of modelled wind speed distribution. The *top three figures* show the shape parameter κ (–), the *bottom three figures* show the scale parameter λ (m s^{-1}). From left two right, figures show the 1957–2011 annual average, winter (DJF) average and summer (JJA) average

effect is observed and a relatively low shape parameter is found. The resultant pattern in northern Greenland shows three large regions of high κ, separated by regions of somewhat lower κ due to convex topography. Furthermore, several smaller scale regions of high κ are found, for example the drainage basin of Inglefield Fjord (77.5°N, 65°W). As expected, the shape parameter, being a rough measure of the forcing mechanisms of the wind, follows the yearly cycle of the katabatic forcing. Over the ocean, katabatic forcing is absent and the seasonal cycle reflects changes of thermal wind and large scale forcing instead. Over Baffin Bay to the west of Greenland a thermal jet is present in winter, which represents a relatively constant forcing and associated higher (2.5–3) values of the shape parameter. In summer, reduced sea ice concentrations and reduced cold air drainage from the ice sheet limit the

accumulation of cold air in this region and reduce thermal forcing. As a consequence, large scale forcing is more important and a lower shape parameter results.

Figure 9 highlights the linear trends of the Weibull parameters over the period 1990–2011. Monthly values of the Weibull parameters were calculated from daily average data, and used to create annual, winter and summer averages. Regions where trends are significant at the 95 % level are dotted. Significance of these trends was corrected if a significant (>95 %) serial correlation was found using the methods presented in Santer et al. (2000).

Trends in the parameters are generally small, while substantial interannual variability exists, resulting in few significant trends. The yearly average scale parameter λ decreases over the entire ice sheet between 1990 and 2011, except in a very narrow band over the ablation zone in the southwest. Since the scale parameter is closely related to the average wind speed, this suggests a reduction of the dominant katabatic forcing, and hence of the potential temperature deficit over most of the ice sheet. Over the steep coastal slopes, where the katabatic and thermal forcing are both large and opposite, an increase in net forcing may explain the simulated modest increase of wind speed. The katabatic forcing depends linearly on the potential temperature deficit, while the thermal forcing depends on horizontal gradients of the vertically integrated potential temperature deficit. It can therefore be expected that both forcings are unevenly reduced, apparently leading to an increased net forcing in this region. The shape parameter does not show an clear decrease over the ice sheet, as might be expected in response to declining katabatic forcing. However, since the 1990s there have been changes in the general atmospheric circulation which may influence the observed changes of the shape parameter (Fettweis et al. 2012b).

In summer, wind speeds decrease over most of the ice sheet, as indicated by a decrease of the scale parameter λ. The relatively uniform pattern of wind speed decrease over the ice sheet suggests a decrease in katabatic forcing, while the lack of a clear pattern of the shape parameter suggests a change of synoptic influence as well. Over coastal regions where melt occurs, a increase of both wind speed and the shape parameter is observed in summer. Here, increased melt rates cause an increased downward sensible heat flux and resulting katabatic forcing.

The strong negative trend in wind speed over the Greenland Sea may be related to a decline of the thermal forcing following a decline in sea ice extent. A decline of sea ice cover increases the heat exchange between the atmosphere and ocean and therefore limits cold air pooling and associated thermal winds. This effect is strongest in winter, but persists throughout the year.

3.3 Projected changes of the wind climate

To investigate future changes of the wind climate, RACMO2 is forced at the lateral boundaries by simulations from the GCM HadGEM2-ES from the UK Met Office. HadGEM2 is chosen because it is one of the best GCMs of the 5th Coupled Model Intercomparison Project (CMIP5) in reproducing the large scale circulation as given by the ECMWF reanalyses, and the best of all over the Greenland ice sheet (Fettweis et al. 2012a). The atmosphere is too warm in summer in HadGEM2, which is problematic for surface mass balance estimates. Here, we limit ourselves to the wind climate, and this model deficiency is likely of limited importance. Indeed, the simulated near-surface wind field from the HadGEM2 forced run shows minimal deviations from the observationally forced run (see Online Resources).

To investigate the response of the surface wind climate of the GrIS to further sustained atmospheric warming, we compare model output from 1981 to 1998 with output from 2081 to 2098. RACMO2 was forced with HadGEM2 simulations which were forced with a scenario of mid-range warming and radiative forcing of +4.5 W m^{-2} in 2100. A temperature increase over the ice sheet is observed in response to this forcing that is statistically significant at the 99 % level everywhere. The smallest temperature change is found over the southeastern coast where temperatures rise roughly 3 K (see Online Resources). Over the central ice sheet a 5 K temperature changes is observed with maxima of over 6 K over the northern tundra and the sea ice covered area of the Greenland sea. Over the Arctic ocean north of the GrIS temperature increases are as high as 9 K.

Figure 10 shows the average change of the Weibull parameters between 1981–1998 and 2081–2098. The scale parameter λ indicates that annually averaged wind speeds decrease over the entire ice sheet, except in a band along the coast. At the same time, a reduction of the shape parameter κ is observed. This pattern is similar to the recent trend from Fig. 9, and we maintain our conclusion that reduced katabatic forcing is the dominant cause of this pattern in the interior of the GrIS, while an uneven reduction of katabatic and thermal forcing is the cause of the wind speed increase over the coastal regions. This conclusion is supported by the modelled change of the surface potential temperature deficit (Fig. 11), which shows a decrease in strength over the entire ice sheet in all seasons except summer. Furthermore, the decrease of the potential temperature deficit over the sea ice region is stronger than over the ice sheet, and so the thermal gradient between the two is reduced. In fact, analysis of the integrated potential temperature deficit shows an increase of the integrated deficit over the ice sheet, and a reduction

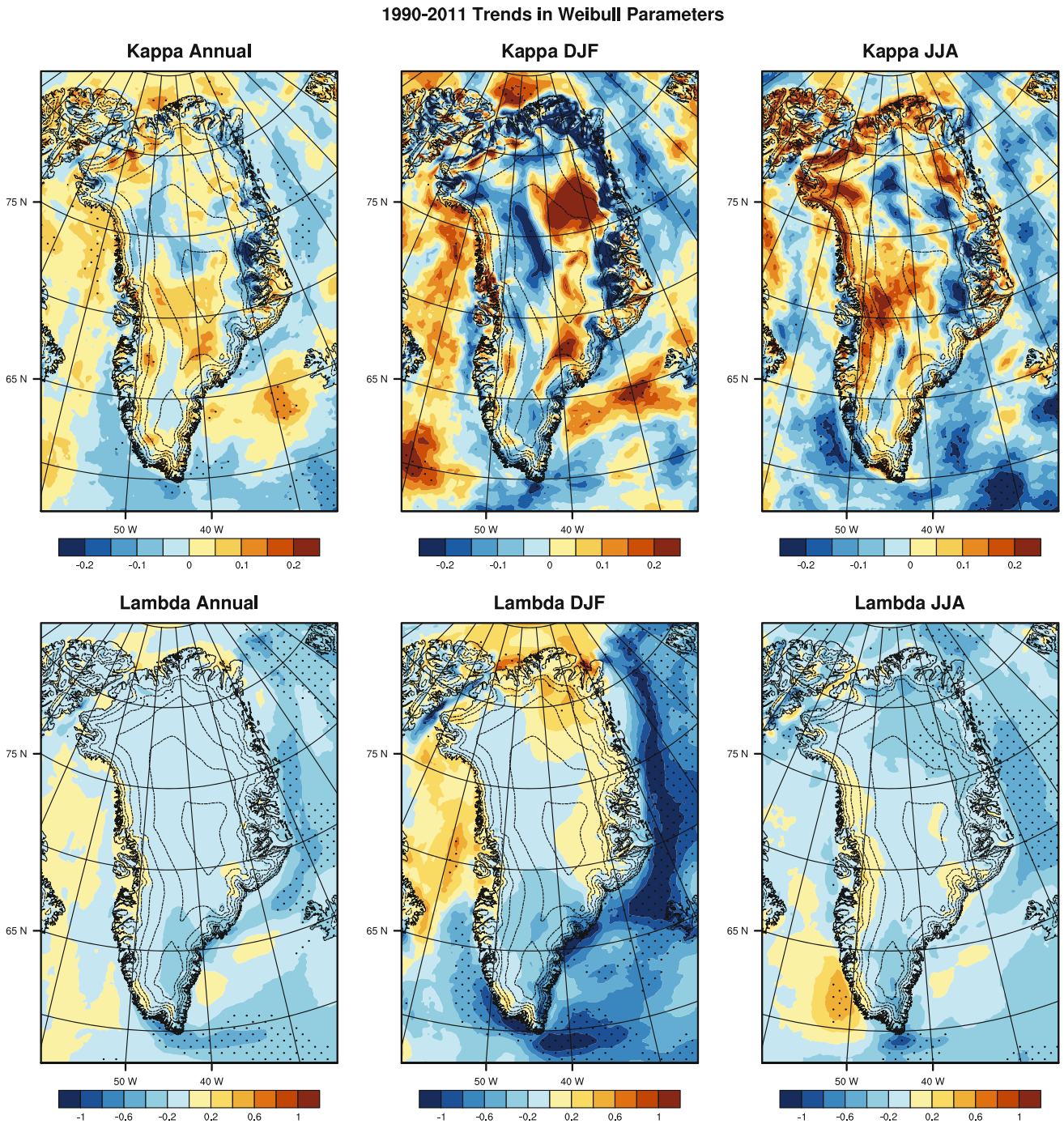

Fig. 9 Modelled linear trends of Weibull parameters over the period 1990–2011, given in units of dec^{-1} for κ (*top*) and m $s^{-1}dec^{-1}$ for λ (*bottom*). The Weibull distribution was fitted to daily average data for all months in the modelled period. Annual averages (*left*), winter (DJF) averages and summer (JJA) averages were taken for every year, after which a linear trend was calculated

over the sea ice region, confirming the decrease of the thermal forcing.

The decrease of the potential temperature deficit also affects the higher elevation parts of the ice sheet in summer (Fig. 11), suggesting that the potential temperature deficit decreases over snow surfaces at subfreezing temperatures. The temperature deficit layer is created by a sensible heat flux from the air to the surface that depends on the temperature difference between them. At subfreezing temperatures an increase of near-surface temperature will be accompanied by an increase of surface layer snow temperature. Possibly positive temperature albedo feedbacks in

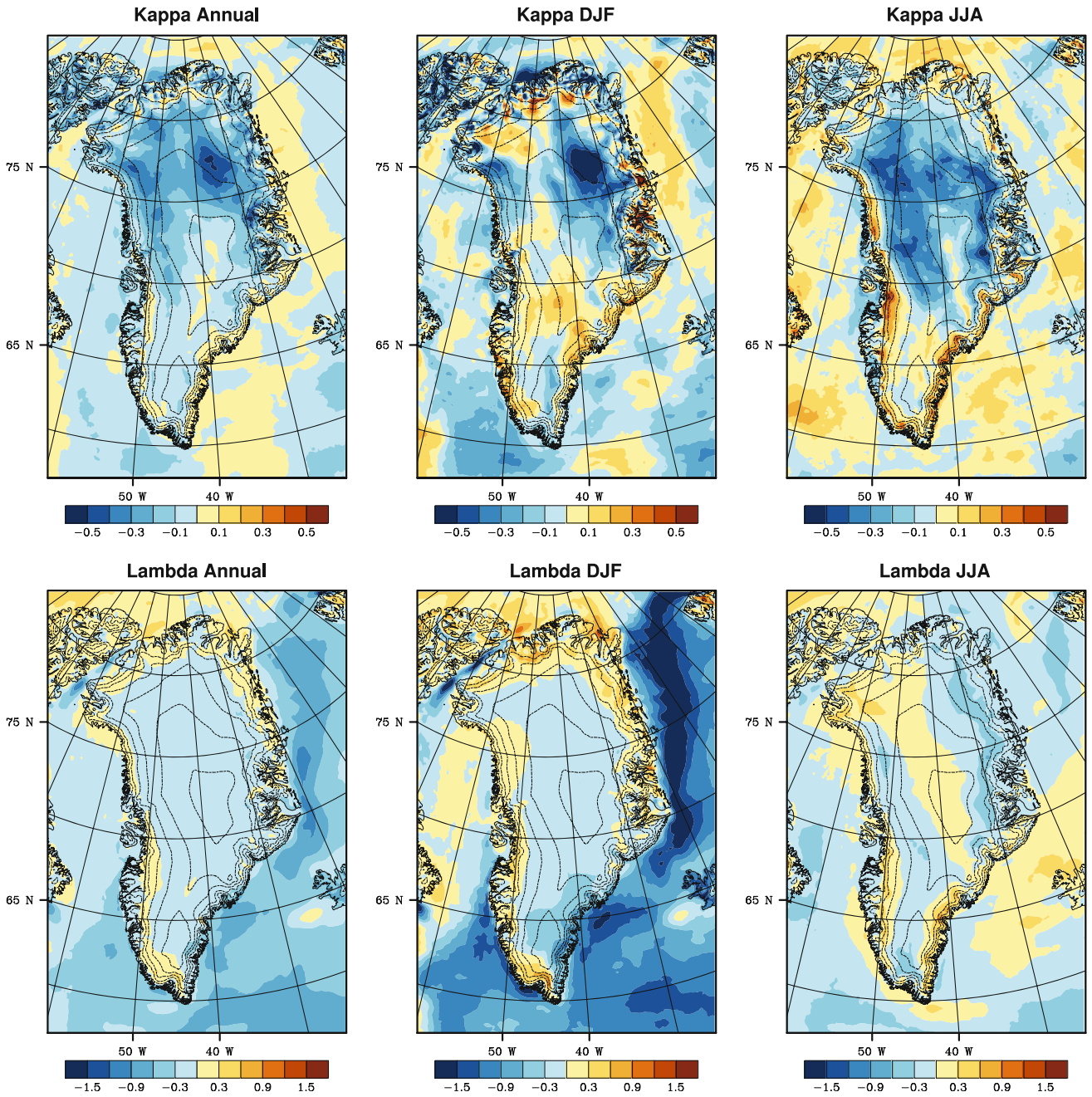

Fig. 10 Average change of the Weibull shape parameter (*top*) and scale parameter (*bottom*) between 1981–1998 and 2081–2098 for selected seasons

the snowpack have enhanced the warming of the snow surface such that the temperature difference with the overlying air is reduced.

Over the ablation zone, the surface temperature cannot rise above freezing in summer, and a stronger temperature gradient between surface and atmosphere will create a larger potential temperature deficit, such that katabatic forcing increases over the ablation zone (Fig. 11). The associated increase of the scale parameter is clearly visible over the coastal regions in southern Greenland in summer (Fig. 10). Because the near-surface air temperature over the ablation zone is limited by the surface temperature, it warms less than near-surface air over the tundra. The contrast between the ablation zone and the tundra and ocean is enlarged. The increasing wind speed of tip jets and barrier winds along the southwestern coast may partly be related to this effect. Franco et al. (2013) found a similar increase of near-surface winds using the regional climate model MAR.

Interestingly, largest changes of the wind are observed over the oceans surrounding the GrIS. Particularly the

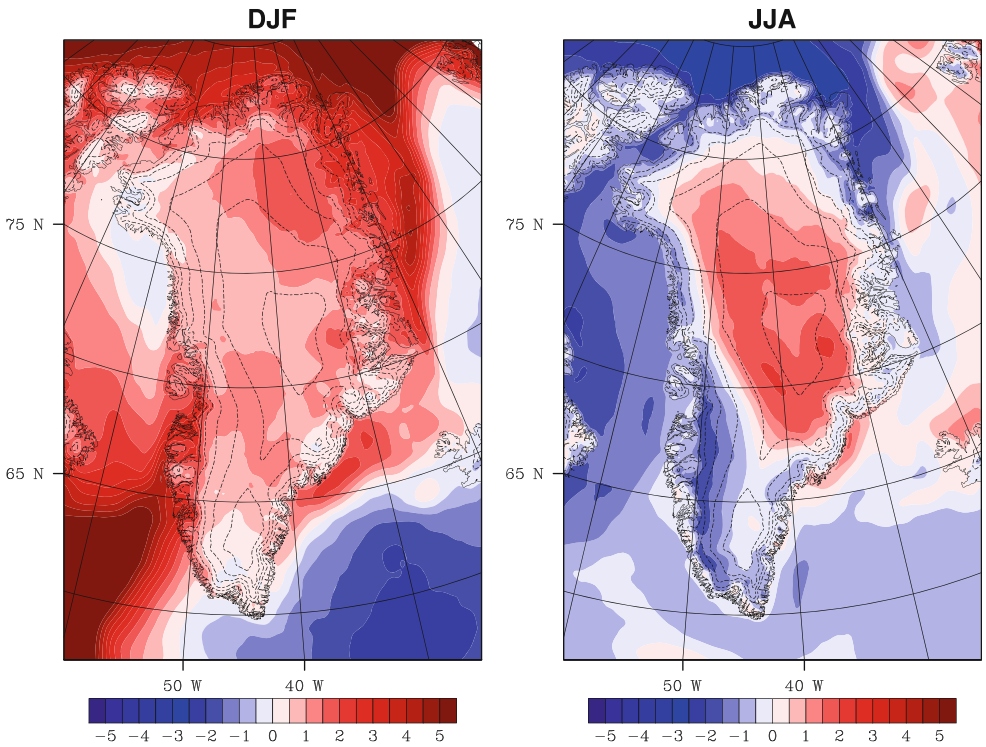

Fig. 11 Difference in average surface potential temperature deficit (K) for the period 2081–2098 compared to the period 1981–1998. Winter (*left*) and summer (*right*) are shown

northerly Greenland Sea Jet to the northeast of the ice sheet substantially reduces in strength by up to 2.5 m s^{-1} in winter. This change is caused by a strong decline of the thermal forcing, which is likely related to declining sea ice extent. Changes of the wind further to the south are related to changes in large scale forcing and thermal effects. However, changes of the large scale forcing are likely limited, as HadGEM2 simulations do not show a significant change of the large scale circulation (Belleflamme et al. 2012).

4 Conclusions

The wind climate of the Greenland ice sheet is presented using output of the high-resolution RCM RACMO2. The near-surface climate of RACMO2 has been extensively evaluated before, and therefore a limited evaluation focussing on the wind distribution is presented. The quality of the model wind speed distribution is assessed by comparing it to observational data from three AWSs in the ablation zone of southwest Greenland. Performance of the model is good over the ablation zone, and only significantly deviates from observations for location S5 on the tongue of Russell Glacier, a location of complex topography. Wind direction and wind speed are properly represented. The wind distribution is fitted to a Weibull distribution to discriminate between katabatic and synoptically dominated winds.

High values of the shape parameter ($\kappa > 4$) are indicative of katabatic forced winds and are found over most of the ice sheet, except in the south where considerable synoptic influence is found. Extremely high values of the shape parameter ($\kappa > 5$) are found in regions of concave topography over the northern part of the ice sheet where confluence of already strong katabatic wind occurs. The drainage basin of these winds is enlarged in these regions while adiabatic heating is suppressed, leading to strong, persistent and constant katabatic winds. Low values of the shape parameter are found in bands along the southwestern and southeastern coast, where strong barrier winds occur. The large scale circulation forces cold winds from the ice sheet against the steep topography where a pool of cold air builds up, leading to strong thermal forcing. The value of κ in this region clearly reveals the dominance of the katabatic forcing in winter, whereas summer values are more indicative of synoptic influence.

Trends of the Weibull parameters are investigated to reveal changes in the wind climate in response to observed atmospheric warming over the GrIS. A reduction of the katabatic forcing decreases wind speeds over the ice sheet during the cold season. Over steep topography at the ice sheet margin an increase of the wind is observed because the opposite thermal and katabatic forcings are unevenly reduced. Due to the short time series and high interannual variability, most observed trends are not statistically significant at the 95 % confidence level. More distinct patterns of change are found in a comparison of simulations from

1981–1998 with 2081–2098. Again, a decrease of wind speed is observed over the central ice sheet, whereas wind speeds increase over the ice sheet margin. Of particular importance is the strong reduction of the thermally forced northerly Greenland Sea Jet. A reduction of wind speeds of up to 2.5 m s^{-1} is observed in winter, likely in response to declining sea ice cover and associated with less pronounced cold air pooling. Since this jet is the dominant mechanism of sea ice transport into the North Atlantic through Fram Strait, this represents a positive feedback on the sea ice cover near the GrIS. In summer, winds decrease over the high elevation portions of the ice sheet in response to decreased katabatic forcing, whereas winds increase over the melting zone. There, near-surface air temperatures increase while the surface is limited to the melting point. The stronger resulting sensible heat flux increases the katabatic forcing of the wind.

The findings of this research reveal a particularly important role of sea ice in controlling the circulation over the Greenland Sea. Modelling sea ice in RCMs, rather than prescribing it, is a promising topic for future research. The role of the large scale circulation in driving future changes also requires further study. Finally, this research shows the importance of local boundary layer forcing to the wind climate of Greenland, hinting at the need of even higher-resolution models to capture local variability.

References

Bamber JL, Layberry RL, Gogineni SP (2001) A new ice thickness and bed data set for the Greenland ice sheet: 1. Measurement, data reduction, and errors. J Geophys Res 106(D24):33773–33780. doi:10.1029/2001JD900054

Belleflamme A, Fettweis X, Lang C, Erpicum M (2012) Current and future atmospheric circulation at 500 hPa over Greenland simulated by the CMIP3 and CMIP5 global models. Clim Dyn. doi:10.1007/s00382-012-1538-2

Bøggild CE, Brandt RE, Brown KJ, Warren SG (2010) The ablation zone in northeast Greenland: ice types, albedos and impurities. J Glaciol 56:101–113. doi:10.3189/002214310791190776

Bougamont M, Bamber JL, Greuell W (2005) A surface mass balance model for the Greenland ice sheet. J Geophys Res 110(F04018). doi:10.1029/2005JF000348

Box J, Bromwich D, Veenhuis B, Bai L, Stroeve J, Rogers J, Steffen K, Haran T, Wang S (2006) Greenland ice sheet surface mass balance variability (1988–2004) from calibrated Polar MM5 output. J Clim 19:2783–2800. doi:10.1175/JCLI3738.1

Box JE, Yang L, Bromwich DH, Bai LS (2009) Greenland ice sheet surface air temperature variability: 1840-2007. J Clim 22:4029–4049. doi:10.1175/2009JCLI2816.1

Bromwich DH, Cassano JJ, Klein T, Heinemann G, Hines KM, Steffen K, Box JE (2001) Mesoscale modeling of katabatic winds over Greenland with the Polar MM5. Mon Weather Rev 129:2290–2309. doi:10.1175/1520-0493(2001)129<2290:MMOKWO>2.0.CO;2

Cappelen J, Jørgensen BV, Laursen EV, Stannius LS, Thomsen RS (2001) The observed climate of Greenland, 1958–1999—with climatological standard normals, 1961–1990. Technical report 00-18, Danish Meteorological Institute, Ministery of Transport, Copenhagen, Denmark

Cassano JJ, Box JE, Bromwich DH, Li L, Steffen K (2001) Evaluation of Polar MM5 simulations of Greenlands's atmospheric circulation. J Geophys Res 106(D24):33867–33889. doi:10.1029/2001JD900044

Dee DP, Uppala SM, Simmons AJ, Berrisford P, Poli P, Kobayashi S, Andrae U, Balmaseda MA, Balsamo G, Bauer P, Bechtold P, Beljaars ACM, van de Berg L, Bidlot J, Bormann N, Delsol C, Dragani R, Fuentes M, Geer AJ, Haimberger L, Healy SB, Hersbach H, Hlm EV, Isaksen L, Kllberg P, Khler M, Matricardi M, McNally AP, Monge-Sanz BM, Morcrette JJ, Park BK, Peubey C, de Rosnay P, Tavolato C, Thpaut JN, Vitart F (2011) The ERA-Interim reanalysis: configuration and performance of the data assimilation system. Q J R Meteor Soc 137(656):553–597. doi:10.1002/qj.828

Dethloff K, Schwager M, Christensen J, Kiilholm S, Rinke A, Dorn W, Jung-Rothenhäusler F, Fischer H, Kipfstuhl S, Miller H (2002) Recent Greenland accumulation estimated from regional climate model simulations and ice core analysis. J Clim 15:2821–2832. doi:10.1175/1520-0442(2002)015<2821:RGAEFR>2.0.CO;2

Duynkerke PG, van den Broeke MR (1994) Surface energy balance and katabatic flow over glacier and tundra during GIMEX-91. Global Planet Change 9:17–28. doi:10.1016/0921-8181(94)90004-3

Ettema J, van den Broeke MR, van Meijgaard E, van de Berg WJ, Bamber JL, Box JE, Bales RC (2009) Higher surface mass balance of the Greenland ice sheet revealed by high-resolution climate modeling. Geophys Res Lett 36(L12501). doi:10.1029/2009GL038110

Ettema J, van den Broeke MR, van Meijgaard E, van de Berg WJ (2010a) Climate of the Greenland ice sheet using a high-resolution climate model—part 2: near-surface climate and energy balance. Cryosphere 4:529–544. doi:10.5194/tc-4-529-2010

Ettema J, van den Broeke MR, van Meijgaard E, van de Berg WJ, Box JE, Steffen K (2010b) Climate of the Greenland ice sheet using a high-resolution climate model—part 1: evaluation. Cryosphere 4:511–527. doi:10.5194/tc-4-511-2010

Fettweis X, Franco B, Tedesco M, van Angelen JH, Lenaerts JTM, van den Broeke MR, Galée H (2012a) Estimating Greenland ice sheet surface mass balance contribution to future sea level rise using the regional atmospheric climate model MAR. Cryosphere Discuss 6:3101–3147. doi:10.5194/tcd-6-3101-2012

Fettweis X, Hanna E, Lang C, Belleflamme A, Erpicum M, Gallée H (2012b) Brief communication "Important role of the mid-tropospheric atmospheric circulation in the recent surface melt increase over the Greenland ice sheet". Cryosphere Discuss 4101–4122. doi:10.5194/tcd-6-4101-2012

Franco B, Fettweis X, Lang C, Erpicum M (2012) Impact of spatial resolution on the modelling of the Greenland ice sheet surface mass balance between 1990–2010, using the regional climate model MAR. Cryosphere 6(3):695–711. doi:10.5194/tc-6-695-2012

Franco B, Fettweis X, Erpicum M (2013) Future projections of the Greenland ice sheet energy balance driving the surface melt. Cryosphere 7:1–18. doi:10.5194/tc-7-1-2013

Gallée H, Schayes G (1994) Development of a three-dimensional meso-γ primitive equation model: Katabatic winds simulation in the area of Terra Nova Bay, Antarctica. Mon Weather Rev 122:671–685. doi:10.1175/1520-0493(1994)122<0671:DOATDM>2.0.CO;2

Harden BE, Renfrew IA (2012) On the spatial distribution of high winds off southeast Greenland. Geophys Res Lett 39(L14806). doi:10.1029/2012GL052245

Heinemann G (1999) The KABEG'97 field experiment: an aircraft-based study of katabatic wind dynamics over the Greenland ice sheet. Bound Lay Meteorol 93:75–116. doi:10.1023/A:1002009530877

Heinemann G, Klein T (2002) Modelling and observations of the katabatic flow dynamics over Greenland. Tellus A 54:542–554. doi:10.1034/j.1600-0870.2002.201401.x

Isemer H, Hasse L (1991) The scientific Beaufort equivalent scale: effects on wind statistics and climatological air-sea flux estimates in the North Atlantic ocean. J Clim 4:819–836. doi:10.1175/1520-0442(1991)004<0819:TSBESE>2.0.CO;2

Klein T, Heinemann G, Bromwich DH, Cassano JJ, Hines KM (2001) Mesoscale modeling of katabatic winds over Greenland and comparisons with AWS and aircraft data. Meteorol Atmos Phys 78:115–132. doi:10.1007/s007030170010

Kuipers Munneke P, Van den Broeke MR, Lenaerts JTM, Flanner MG, Gardner AS, Van de Berg WJ (2011) A new albedo parameterization for use in climate models over the Antarctic ice sheet. J Geophys Res 116(D05114). doi:10.1029/2010JD015113

Lenaerts JTM, van den Broeke MR, van Angelen JH, van Meijgaard E, Déry SJ (2012a) Drifting snow climate of the Greenland ice sheet: a study with a regional climate model. Cryosphere 6:891–899. doi:10.5194/tc-6-891-2012

Lenaerts JTM, van den Broeke MR, van de Berg WJ, van Meijgaard E, Kuipers Munneke P (2012b) A new, high-resolution surface mass balance map of Antarctica (1979–2010) based on regional atmospheric climate modelling. Geophys Res Lett 39(L04501). doi:10.1029/2011GL050713

Monahan AH (2006a) The probability distribution of sea surface wind speeds. part I: theory and SeaWinds observations. J Clim 19:497–520. doi:10.1175/JCLI3640.1

Monahan AH (2006b) The probability distribution of sea surface wind speeds. Part II: dataset intercomparison and seasonal variability. J Clim 19:521–534. doi:10.1175/JCLI3641.1

Moore GWK, Renfrew IA (2005) Tip jets and barrier winds: a QuikSCAT climatology of high wind speed events around Greenland. J Clim 18:3713–3725. doi:10.1175/JCLI3455.1

Moss RH, Edmonds JA, Hibbard KA, Manning MR, Rose SK, Van Vuuren DP, Carter TR, Emori S, Kainuma M, Kram T, Meehl GA, Mitchell JFB, Nakicenovic N, Riahi K, Smith SJ, Stouffer RJ, Thomson AM, Weyant JP, Wilbanks TJ (2010) The next generation of scenarios for climate change research and assessment. Nature 463:747–756. doi:10.1038/nature08823

Oerlemans J, Vugts HF (1993) A meteorological experiment in the melting zone of the Greenland ice sheet. B Am Meteorol Soc 74(3):355–365. doi:10.1175/1520-0477(1993)074<0355:AMEITM>2.0.CO;2

Parish TR, Bromwich DH (1987) The surface windfield over the Antarctic ice sheets. Nature 328:51–54. doi:10.1038/328051a0

Pavia EG, O'Brien JJ (1986) Weibull statistics of wind speed over the ocean. J Clim Appl Meteorol 25:1324–1332. doi:10.1175/1520-0450(1986)025<1324:WSOWSO>2.0.CO;2

Pryor SC, Barthelmie RJ, Kjellström E (2005) Potential climate change impact on wind energy resources in northern Europe: analyses using a regional climate model. Clim Dyn 25:815–835. doi:10.1007/s00382-005-0072-x

Renfrew IA, Anderson PS (2002) The surface climatology of an ordinary katabatic wind regime in Coats Land, Antarctica. Tellus A 54:463–484. doi:10.1034/j.1600-0870.2002.201397.x

Rignot E, Velicogna I, van den Broeke MR, Monaghan A, Lenaerts JTM (2011) Acceleration of the contribution of the Greenland and Antarctic ice sheets to sea level rise. Geophys Res Lett 38(L05503). doi:10.1029/2011GL046583

Santer BD, Wigley TML, Boyle JS, Gaffen DJ, Hnilo JJ, Nychka D, Parker DE, Taylor KE (2000) Statistical significance of trends and trend differences in layer-average atmospheric temperature time series. J Geophys Res 105(D6):7337–7356. doi:10.1029/1999JD901105

Sanz Rodrigo J, Buchlin JM, Van Beeck J, Lenaerts JTM, Van den Broeke MR (2012) Evaluation of Antarctic surface wind climate from ERA reanalyses and RACMO2/ANT simulations based on automatic weather stations. Clim Dyn. Online first. doi:10.1007/s00382-012-1396-y

Steffen K, Box JE (2001) Surface climatology of the Greenland ice sheet: Greenland Climate Network 1995–1999. J Geophys Res 106(D24):33951–33964. doi:10.1029/2001JD900161

Undén P, Rontu L, Järvinen H, Lynch P, Calvo J, Cats G, Cuxart J, Eerola K, Fortelius C, Garcia-Moya JA, Jones C, Lenderlink G, Mcdonald A, Mcgrath R, Navascues B, Nielsen NW, Ødegaard V, Rodriguez E, Rummukainen M, Rõõm R, Sattler K, Sass BH, Savijärvi H, Schreur BW, Sigg R, The H, Tijm A (2002) HIRLAM-5 scientific documentation. Tech. rep., Swedish Meteorological and Hydrological Institute, Norrköping, Sweden

Våge K, Spengler T, Davies HC, Pickart RS (2009) Multi-event analysis of the westerly Greenland tip jet based upon 45 winters in ERA-40. Q J R Meteorol Soc 135:1999–2011. doi:10.1002/qj.488

Van Angelen JH, Van den Broeke MR, Van de Berg WJ (2011a) Momentum budget of the atmospheric boundary layer over the Greenland ice sheet and its surrounding seas. J Geophys Res 116(D10101). doi:10.1029/2010JD015485

Van Angelen JH, Van den Broeke MR, Kwok R (2011b) The Greenland Sea Jet: a mechanism for wind-driven sea ice export through Fram Strait. Geophys Res Lett 38(L12805). doi:10.1029/2011GL047837

Van Angelen JH, Lenaerts JTM, Lhermitte S, Fettweis X, Kuipers Munneke P, Van den Broeke MR, Van Meijgaard E (2012) Sensitivity of Greenland ice sheet surface mass balance to surface albedo parameterization: a study with a regional climate model. Cryosphere Discuss 6:1531–1562. doi:10.5194/tcd-6-1531-2012

Van As D, Fausto R, PROMICE project team (2011) Programme for monitoring of the Greenland ice sheet (PROMICE): first temperature and ablation recors. Geol Surv Den Greenl 23:73–76

Van de Berg WJ, Van den Broeke MR, Van Meijgaard E (2008) Spatial structures in the heat budget of the Antarctic atmospheric boundary layer. Cryosphere 2(1):1–12. doi:10.5194/tc-2-1-2008

Van de Wal RSW, Boot W, Smeets CJPP, Snellen H, van den Broeke MR, Oerlemans J (2012) Twenty-one years of mass balance observations along the K-transect, West Greenland. Earth Syst Sci Data 4(1):31–35. doi:10.5194/essd-4-31-2012

Van den Broeke MR, Gallée H (1996) Observation and simulation of barrier winds at the western margin of the Greenland ice sheet. Q J R Meteor Soc 122:1265–1383. doi:10.1002/qj.49712253407

Van den Broeke MR, Van Lipzig NPM (2003) Factors controlling the near-surface wind field in Antarctica. Mon Weather Rev 131:733–743. doi:10.1175/1520-0493(2003)131<0733:FCTNSW>2.0.CO;2

Van den Broeke MR, Duynkerke PG, Oerlemans J (1994) The observed katabatic flow at the edge of the Greenland ice sheet during GIMEX-91. Global Planet Change 9:3–15. doi:10.1016/0921-8181(94)90003-5

Van den Broeke MR, Smeets P, Ettema J (2008a) Surface layer climate and turbulent exchange in the ablation zone of the west Greenland ice sheet. Int J Climatol 29:2309–2323. doi:10.1002/joc.1815

Van den Broeke MR, Smeets P, Ettema J, Kuipers Munneke P (2008b) Surface radiation balance in the ablation zone of the west Greenland ice sheet. J Geophys Res 113(D13105). doi:10.1029/2007JD009283

Van den Broeke MR, Bamber J, Ettema J, Rignot E, Schrama E, Van de Berg WJ, Van Meijgaard E, Velicogna I, Wouters B (2009)

Partitioning recent Greenland mass loss. Science 326:984–986. doi:10.1126/science.1178176

Van Meijgaard E, Van Ulft LH, Van de Berg WJ, Bosveld FC, Van den Hurk BJJM, Lenderink G, Siebesma AP (2008) The KNMI regional atmospheric climate model RACMO version 2.1. Technical Report TR-302, Royal Netherlands Meteorological Institute, De Bilt, The Netherlands

White P (2001) Physical processes (CY23R4). Technical report, European Centre for Medium-Range Weather Forecasts (ECMWF)